Dalton Transactions

ROYAL SOCIETY OF CHEMISTRY

PAPER

View Article Online
View Journal | View Issue

Cite this: *Dalton Trans.*, 2025, **54**, 11725

Homoleptic copper(I)–bisphosphine complexes as photoredox catalysts†

Priya Saha, [a] Ryunosuke Tomita,‡[b] Takao Tsuneda, ‡[a] Pingyu Jiang, [a] Tetsuya Taketsugu,[a,c] Mingoo Jin [a,d] and Dennis Chung-Yang Huang *[a]

Received 9th May 2025,
Accepted 5th July 2025

DOI: 10.1039/d5dt01099c

rsc.li/dalton

Copper photoredox catalysis has emerged as a practical methodology in organic synthesis, with tetracoordinate copper complexes playing a central role. Among these, homoleptic complexes bearing two bisimine ligands (**CuN4**) and heteroleptic complexes containing one bisimine and one bisphosphine ligand (**CuN2P2**) are the most utilized. In contrast, homoleptic copper–bisphosphine complexes (**CuP4**) have received comparatively less attention, despite their recent involvement in novel synthetic transformations. Herein, we report a systematic study of this underexplored family of copper complexes. Representative **CuP4** complexes were synthesized, and their photophysical and electrochemical properties were characterized. Their photocatalytic activity was demonstrated in representative coupling reactions. The results provide insights for guiding future ligand design to develop more active copper-based photocatalysts.

Introduction

In the past decades, the field of photoredox catalysis has been significantly enriched by the incorporation of base metal catalysts, where earth-abundant metals complexed with suitable ligands are employed as photocatalysts.[1] In addition to being cost-effective, this new family introduces the merit of tunability that iridium-, ruthenium-, or organic-based photocatalysts cannot achieve. The choice of ligands often imparts modulation of photophysical and stereochemical properties of the catalysts, enabling rapid optimization of photocatalytic reactivity *via* screening for a proper combination of metal precursors and ligands. Among all candidates, copper has recently gained broad popularity.[2] Accessibility to Cu(I/II/III) oxidation states allows for engagement with substrates under both photochemical and thermal conditions. As opposed to conventional photocatalysts that are predominantly limited to outer-sphere processes, the flexibility of the ligation fields around the Cu centers resultingly unlocks the inner-sphere mechanism within the same catalytic system. These advantageous characteristics of copper photocatalysts thus render them particularly applicable to organic synthesis, as manifested by the recent wide emergence of Cu–photocatalytic reactions.

To date, tetracoordinate Cu(I) complexes constitute the most widely applied copper photocatalysts (Scheme 1a).[2] Specifically, two classes dominate the field: (i) homoleptic complexes bearing two bisimine ligands (**CuN4**) and (ii) heteroleptic complexes containing one bisimine ligand and another bisphosphine ligand (**CuN2P2**).[3] These photoactive Cu(I) complexes show outstanding responsiveness to visible light and suitable redox properties, allowing them to engage

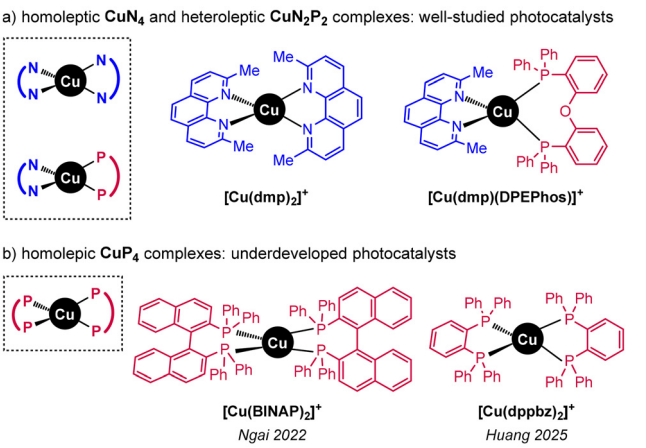

Scheme 1 Tetracoordinate Cu(I) complexes as photocatalysts.

[a]*Institute for Chemical Reaction Design and Discovery (WPI-ICReDD), Hokkaido University, Japan. E-mail: dcyhuang@icredd.hokudai.ac.jp*
[b]*Graduate School of Chemical Sciences and Engineering, Hokkaido University, Japan*
[c]*Department of Chemistry, Faculty of Science, Hokkaido University, Japan*
[d]*List Sustainable Digital Transformation Catalyst Collaboration Research Platform, Institute for Chemical Reaction Design and Discovery (ICReDD List-PF), Hokkaido University, Japan*

†Electronic supplementary information (ESI) available. CCDC 2445749–2445753. For ESI and crystallographic data in CIF or other electronic format see DOI: https://doi.org/10.1039/d5dt01099c

‡Equal contribution.

with a broad range of organic substrates. On the contrary, homoleptic Cu(I)-bisphosphine complexes (**CuP4**) have not received the same level of attention. Although related compounds have been prepared, there exist only scattered reports on their photophysical properties.[4] Furthermore, to the best of our knowledge, applications of these complexes as photocatalysts have not been disclosed until 2022, when the Ngai group demonstrated the effectiveness of $Cu(BINAP)_2^+$ as the photocatalyst in an olefin carbo–aroylation reaction (Scheme 1b).[5] Very recently, our group communicated Cu-catalyzed defluorinative C–O and C–I coupling reactions, where we showed that $Cu(dppbz)_2^+$ can serve as the photocatalyst to reduce trifluoromethylarenes (Scheme 1b).[6] A general mechanism is depicted in Scheme 2, where upon photoirradiation, the excited-state **CuP4** becomes a potent reductant to undergo a single-electron transfer to the substrate (*oxidative quenching*). Mesolytic cleavage of the resulting substrate radical anion then affords a radical intermediate, which can be captured for further transformations. The Cu(II) intermediate can then be reduced to regenerate **CuP4** and close the cycle. The unique role of bisphosphine ligands in enabling these new photocatalytic reactions thus warrants a systematic study of this overlooked class of photoactive complexes.

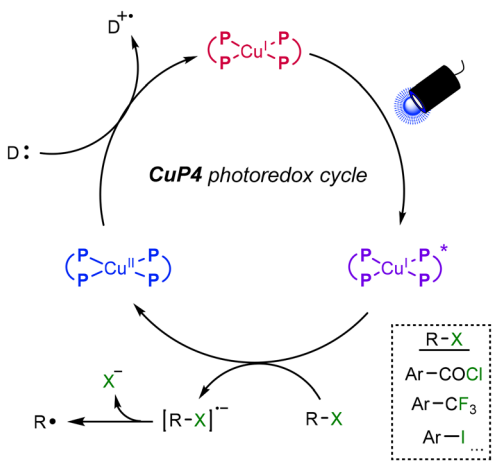

Scheme 2 General catalytic cycle of **CuP4** photocatalysts.

Results and discussion

Preparation of CuP4 complexes

We commenced our studies with the preparation of **CuP4** complexes ligated with representative bisphosphines encompassing a broad range of structural diversity (*e.g.* bite angles: from 83° of dppbz to 112° of XantPhos) (Scheme 3). Utilizing Cu(MeCN)$_4$BF$_4$ as the readily available precursor and the corresponding bisphosphines in 1 : 2 ratio, the desired **CuP4** could be obtained with dppbz, (*R*)-BINAP, BIPHEP, DPEphos, and XantPhos ligands in excellent efficiency (**1–5**). A multigram synthesis of $[Cu(dppbz)_2^+]BF_4^-$ (**1**) was also achieved in 97% yield. The crystal structure of complex **1** and **3**, which were

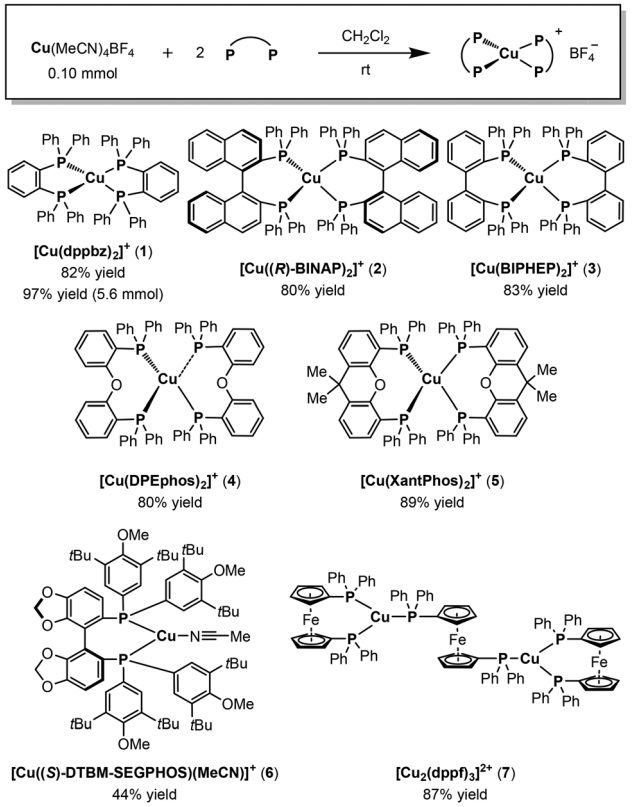

Scheme 3 Synthesis of **CuP4** complexes.

obtained by single crystal XRD measurement, are shown in Fig. 1 (see ESI† for other structures). Notably, certain complexes can display dynamic equilibrium between distinct ligation forms. As has been reported previously, $[Cu(DPEphos)_2^+]$ appears as **CuP3** in the solid-state structure bearing one uncoordinated phosphorus atom, whereas the solution ^{31}P-NMR gives rise to only a single peak.[4d,j] Additionally, $[Cu((R)\text{-}BINAP)_2^+]$ (**2**) exists exclusively as **CuP4** form in $CDCl_3$, but in coordinating CD_3CN, **CuP2** was observed with additional ligated MeCN moieties. In contrast, $[Cu(dppbz)_2^+]$ (**1**) remains as **CuP4** in both $CDCl_3$ and CD_3CN, consistent with its solid-state structure. On the other hand, in the case of (*S*)-DTBM-SEGPHOS, presumably due to its steric bulkiness, a **CuP2** complex (**6**) bearing one acetonitrile ligand was produced. Furthermore, when dppf was used as the ligand, an intriguing dinuclear copper complex (**7**) bridged by a dppf motif was observed in its single crystal structure.[4i] These outcomes showcase how the ligand identity can have a profound influence on the structures of resulting Cu-complexes.

Investigation of CuP4 complexes

Next, we focused our attention on investigating the pertinent properties of five **CuP4** complexes (**1–5**) as photoredox catalysts (Fig. 2). Given their structural stability in chlorinated solvents, the studies were carried out in 1,2-dichloroethane (DCE). In the UV-vis absorption spectra, all complexes exhibit a shoulder peak between 250–350 nm ascribed to MLCT (metal-to-ligand

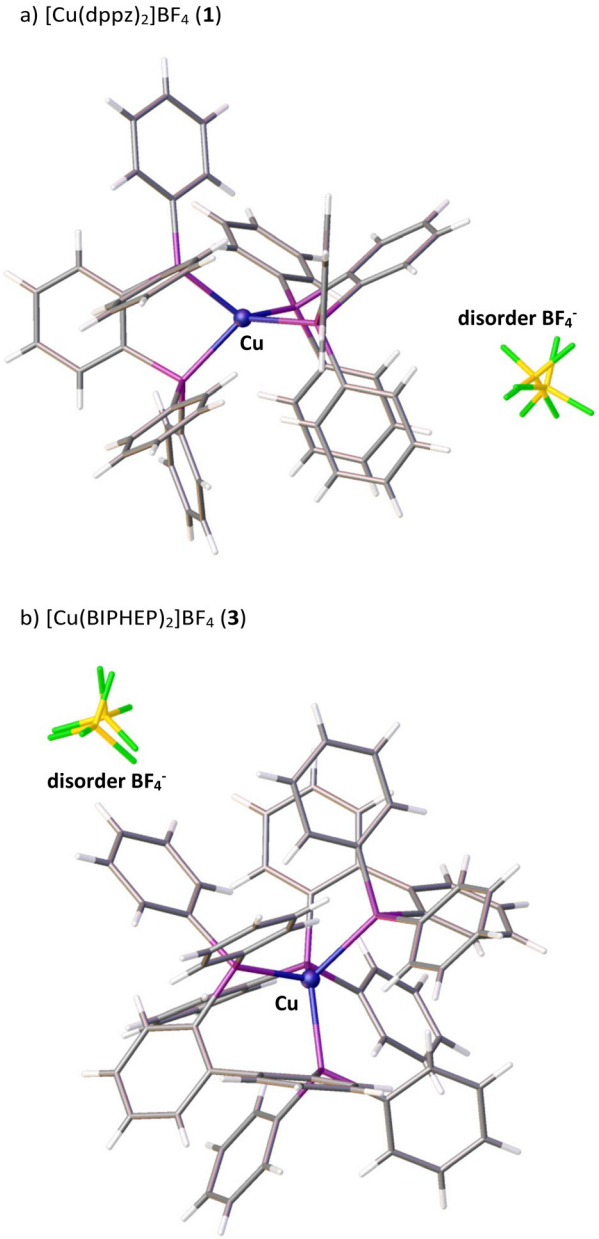

Fig. 1 Crystal structures of Cu-complexes (a) **1** and (b) **3** obtained by single crystal XRD.

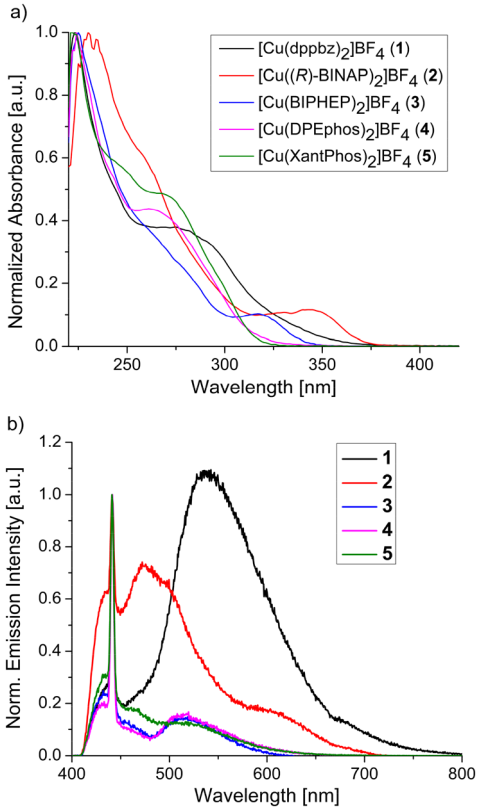

Fig. 2 (a) Absorption spectra and (b) emission spectra (λ_{ex} = 390 nm).

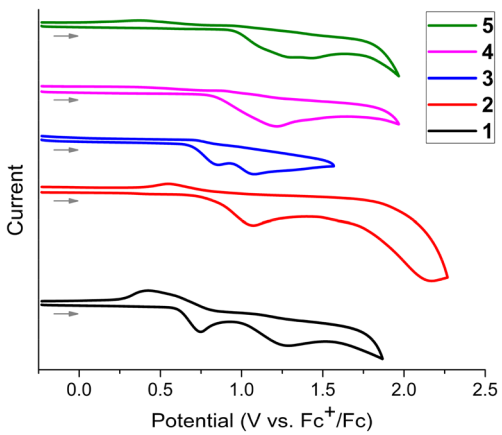

Fig. 3 Cyclic voltammogram and first oxidation potentials of **CuP4** complexes.

charge-transfer) transition, in addition to the most intense ligand-centered π–π* band at 200–250 nm (Fig. 2a). Furthermore, the redox potentials of complexes **1–5** were measured *via* cyclic voltammetry in DCE solvent. Clear anodic peaks in the range of 0.5–1.5 V (*vs.* Fc^+/Fc) were observed in all instances, presumably corresponding to a Cu(I/II) oxidation (Fig. 3). Irreversible peaks can be observed at higher potentials, which may be due to oxidation of phosphine ligands and decomposition of the complexes.[4k]

Upon excitation at 390 nm, multiple peaks could be observed in the emission spectra, noticeably including a broad band at >500 nm (Fig. 2b). Analysis of the emission decay curves revealed that, except for **3**, these long-wavelength bands have decay lifetimes greater than 10 μs, suggesting a sufficiently persistent excited state for substrate engagement (Fig. 4, see ESI† for detailed analysis). Quenching experiments further corroborated this proposal.[7]

Given the intriguingly long decay lifetimes of >500 nm bands in the emission spectra of these **CuP4** complexes, we were interested in probing the triplet states by theoretical

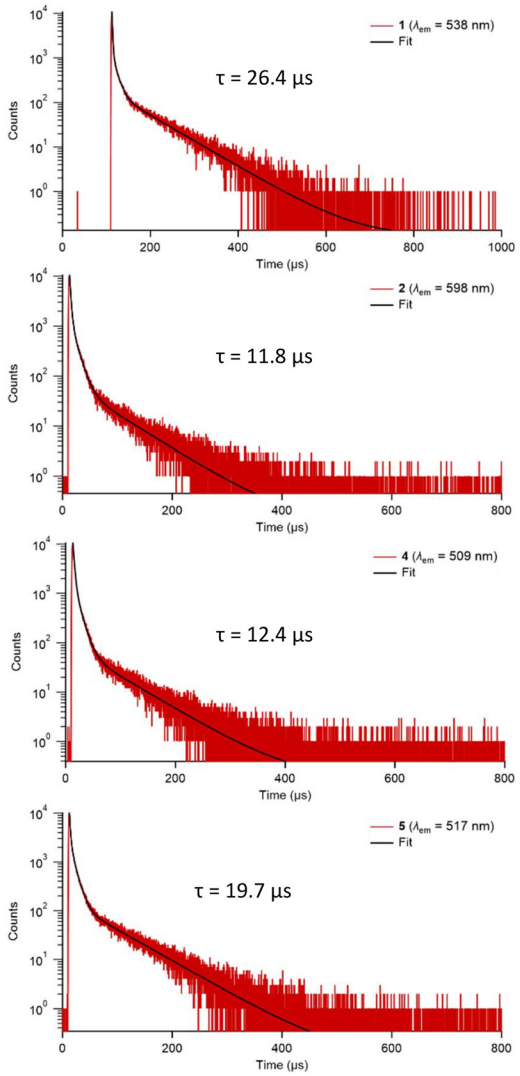

Fig. 4 Emission decay curves of complexes **1**, **2**, **4** and **5**.

approaches. Taken $[Cu(dppbz)_2]^+$ (**1**) as an example, we performed TD-DFT calculations at wB97XD/cc-pVDZ/LanL2DZ(Cu) + CPCM(dichloroethane) level of theory. According to theoretical calculations, the photoinduced process can be interpreted to proceed *via* the following mechanism. First, photoexcitation to the S_1 state corresponds to an MLCT transition (Scheme 4). This leads to a decrease in electron density at the copper center, causing a substantial structural rearrangement from the S_0 geometry to the stable S_1 structure. Concurrently, the oscillator strength decreases markedly, leading to a longer excited-state lifetime. The structural change significantly lowers the S_1 excitation energy, and consequently, the T_1 excitation energy, which involves a similar electronic transition, is also greatly reduced.[8] As a result, upon intersystem crossing from the optimized S_1 structure to the T_1 state, the T_1 excitation energy decreases to 2.44 eV (508 nm). This mechanism is consistent with the experimentally observed broad emission peak ranging from 500 to 700 nm and the 26.4 μs lifetime for

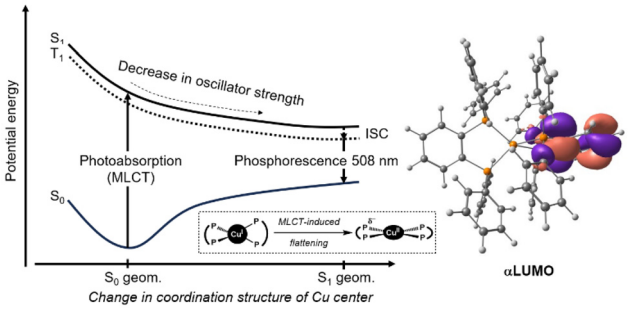

Scheme 4 Electronic transition and structural rearrangement of $[Cu(dppbz)_2]BF_4$ (**1**).

complex **1** and may be the key characteristic responsible for its photoredox activity. Importantly, by combining the computationally obtained triplet energy and experimentally measured ground-state oxidation potential, the excited state reduction potential $E(Cu^{II}/Cu^{I*})$ can be calculated to be −1.35 V (*vs.* SCE).[9] Note that the Ngai group reported a −1.30 V excited state potential for $Cu(BINAP)_2PF_6$ in MeCN.[5]

Synthetic evaluation of CuP4 complexes

Finally, we proceeded to evaluate the photocatalytic activity of these **CuP4** complexes. First, the defluorinative C–I coupling of trifluoromethylarenes was re-examined.[6] We previously proposed that the excited-state **CuP4** served as a reductant to convert $ArCF_3$ into the key $ArCF_2^{\bullet}$ radical intermediate, which then reacts with an "$I^{\bullet}$" equivalent to form an underexplored $ArCF_2I$ class of products. Here, we applied the five isolated **CuP4** and found that $[Cu(dppbz)_2]^+$ (**1**) significantly outperformed other candidates, in accordance with our prior observation (Scheme 5). Furthermore, in the same catalytic system, we established preliminary reactivity for hydrodefluorination and defluoroalkylation, two representative transformations in C–F functionalization (Scheme 6).[10]

Next, hydrodeiodination of aryl iodides, a common model reaction for testing new photocatalysts, was performed (Table 1).[11] In the presence of *tert*-amyl alcohol (*t*-AmOH) and *N*,*N*-diisopropylethylamine (DIPEA), all **CuP4** catalyzed the dehalogenation reaction, where $[Cu(dppbz)_2]^+$ (**1**) again afforded the highest yield (entries 1–5). Conveniently, the same efficiency can be achieved from the *in situ* generated catalyst (entry 6). Control experiments suggest that both *t*-AmOH and DIPEA can potentially serve as the hydrogen

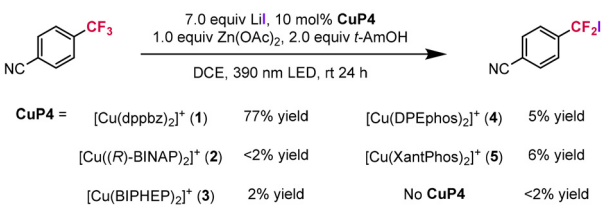

Scheme 5 Defluorinative C–I coupling with $ArCF_3$.

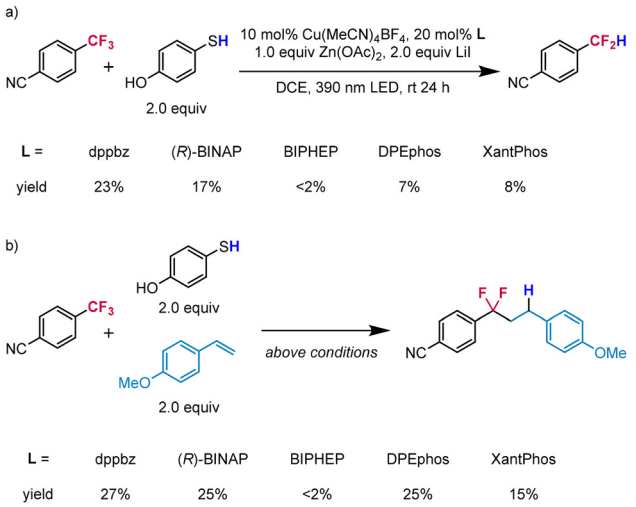

Scheme 6 Hydrodefluorination and defluoroalkylation of $ArCF_3$.

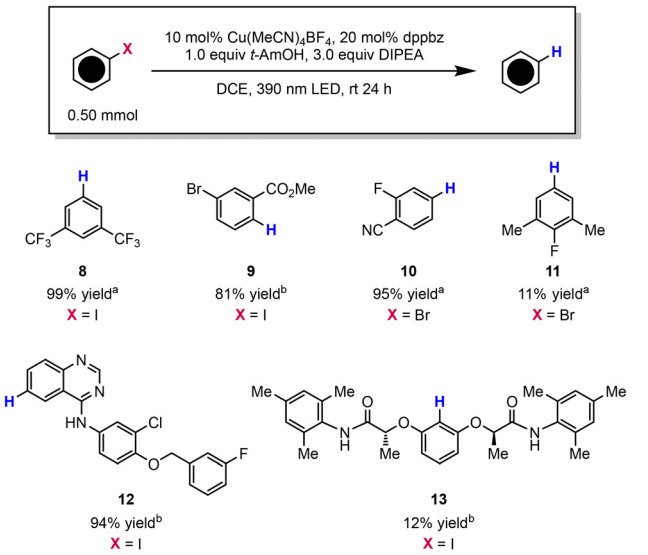

Scheme 7 Scope of photoinduced Cu-catalyzed hydrodehalogenation reactions. [a] Yields determined by ^{19}F-NMR analysis of the crude mixture with (trifluoromethoxy)benzene as the standard. [b] Isolated yields.

Table 1 Photocatalytic hydrodeiodination of aryl iodides

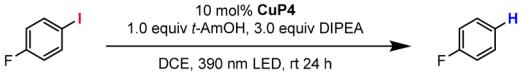

Entry	Conditions	Yield[a] (%)
1	**CuP4** = $[Cu(dppbz)_2]BF_4$ (**1**)	98
2	**CuP4** = $[Cu((R)\text{-BINAP})_2]BF_4$ (**2**)	47
3	**CuP4** = $[Cu(BIPHEP)_2]BF_4$ (**3**)	24
4	**CuP4** = $[Cu(DPEphos)_2]BF_4$ (**4**)	17
5	**CuP4** = $[Cu(XantPhos)_2]BF_4$ (**5**)	35
6	10 mol% $Cu(MeCN)_4BF_4$ + 20 mol% dppbz	>99
7	As entry 6, no *t*-AmOH	72
8	As entry 6, no DIPEA	24
9	As entry 6, no light, rt or 60 °C	<3
10	As entry 6, 440 nm instead of 390 nm LED	15
11	No Cu/L	14

[a] Determined by ^{19}F-NMR analysis of the crude mixture with (trifluoromethoxy)benzene as the standard.

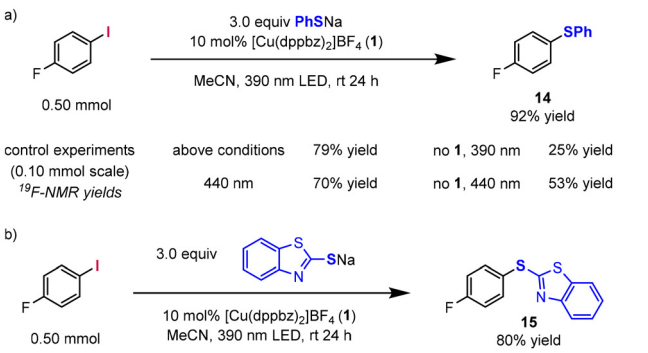

Scheme 8 Photoinduced Cu-catalyzed C–S coupling reactions.

source (entries 7 and 8). Reactions performed in the dark or with 440 nm light resulted in no or diminished yields (entries 9 and 10). On the other hand, an uncatalyzed background reaction proceeded with low efficiency in the absence of copper and ligand (entry 11). A brief scope exploration showed that aryl iodides bearing ester (**9**) or quinazoline (**12**) reacted with high efficiency, but the electron-rich, structurally complex **13** is a less competent substrate (Scheme 7). This protocol is also applicable to aryl bromides, although an electron-poor arene is necessary for higher yield (**10**, **11**). The observed scope where more readily reducible substrates afford higher yields, hints that the reducing power of **CuP4** complexes is the deterministic factor in this transformation.

Lastly, we explored the applicability of complex **1** in photocatalytic C–S coupling (Scheme 8). This transformation is known to proceed through the strategy of electron donor–acceptor (EDA) complex,[12] thus accounting for the significant background reactivity we observed. In the presence of **1**, an improved efficiency was achieved, leading to 92% isolated yield in a 0.50 mmol-scale reaction. The protocol was then successfully applied to the coupling with 2-mercaptobenzothiazole (MBT), a compound used as an accelerant in rubber vulcanization process.

Considering the reduction potentials of substrates examined (*e.g.* E_{red}: *p*-cyanotrifluoromethylbenzene = −1.79 V (ref. 13) and *p*-fluoroiodobenzene = −2.04 V (ref. 14) *vs.* SCE), they do not seem to be reducible by the excited state **CuP4** (E_{red} = −1.35 V for **1**) from the thermodynamic perspective. Substrate preactivation by salt additives as well as the choice of solvent may make up the discrepancy. Coupling the thermodynamically unfavorable electron-transfer step with favorable downstream processes (*e.g.* capture of radical intermediates) may drive the reaction forward. Alternatively, a reductive quenching process may take place, where instead the excited Cu(I) first oxidizes a sacrificial reagent (*e.g.* DIPEA in hydrode-

halogenation reactions).[15] The resultant Cu(0) then carries out the single-electron reduction of substrates. For complex **1**, $E(Cu^{I}/Cu^{0})$ = −2.23 V *vs.* SCE, showing the ability of $[Cu(dppbz)_2]^0$ to reduce most substrates discussed in this section.

Conclusions

In summary, we prepared and investigated five homoleptic Cu(I)-bisphosphine (**CuP4**) complexes. These compounds can be conveniently synthesized from commercially available sources, even up to multigram scale. Spectroscopic and theoretical studies revealed a long-lived, lower-energy T_1 state, and the excited state potential was estimated. We then demonstrated their applicability as photoredox catalysts in three types of coupling reactions, where the Cu-dppbz complex (**1**) stands out in all cases. The superiority of complex **1** can be attributed to its long-lived excited state and suitable redox properties. Based on these understandings, further development in modifying the bisphosphine structures will likely provide more active photocatalysts and expand their synthetic utility to novel chemical transformations.

Author contributions

P. S. conceived the project, synthesized the compounds, performed the photochemical reactions, conducted spectroscopic and electrochemical measurements. R. T. performed the single crystal XRD measurements and assisted the emission decay measurement. T. Tsuneda performed theoretical calculations. P. J. assisted the processing of single crystal XRD and emission decay data. T. Taketsugu assisted the theoretical calculations. M. J. conducted the single crystal XRD analysis and assisted the emission decay measurement. D. C.-Y. H. conceived and managed the project. All authors contributed to the preparation of manuscript.

Conflicts of interest

There are no conflicts to declare.

Data availability

The data supporting this article have been included as part of the ESI.† Crystallographic data for compound **1**, **3**, **4**, **5**, **7** has been deposited at the CCDC under 2445749–2445753.†

Acknowledgements

This work was supported financially by the Institute for Chemical Reaction Design and Discovery (WPI-ICReDD), Hokkaido University, Japanese Government Scholarship (MEXT) for Research Students, JST (FOREST grant JPMJFR232C), List Sustainable Digital Transformation Catalyst Collaboration, and JSPS (JP23K13734). We thank Samuel Jacob for the helpful discussion on electrochemical studies.

References

1 M. L. Clapson, C. S. Durfy, D. Facchinato and M. W. Drover, *Cell Rep. Phys. Sci.*, 2023, **4**, 101548.
2 (*a*) A. Hossain, A. Bhattacharyya and O. Reiser, *Science*, 2019, **364**, eaav9713; (*b*) C. Sandoval-Pauker, G. Molina-Aguirre and B. Pinter, *Polyhedron*, 2021, **199**, 115105; (*c*) J. Beaudelot, S. Oger, S. Peruško, T.-A. Phan, T. Teunens, C. Moucheron and G. Evano, *Chem. Rev.*, 2022, **122**, 16365.
3 (*a*) A. C. Hernandez-Perez and S. K. Collins, *Acc. Chem. Res.*, 2016, **49**, 1557; (*b*) Y. Zhang, M. Schulz, M. Wächtler, M. Karnahl and B. Dietzek, *Coord. Chem. Rev.*, 2018, **356**, 127.
4 (*a*) J. R. Black, W. Levason, M. D. Spicer and M. Webster, *J. Chem. Soc., Dalton Trans.*, 1993, **20**, 3129; (*b*) E. Szłyk, R. Kucharek, I. Szymańska and L. Pazderski, *Polyhedron*, 2003, **22**, 3389; (*c*) A. Tsuboyama, K. Kuge, M. Furugori, S. Okada, M. Hoshino and K. Ueno, *Inorg. Chem.*, 2007, **46**, 1992; (*d*) R. Venkateswaran, M. S. Balakrishna, S. M. Mobin and H. M. Tuononen, *Inorg. Chem.*, 2007, **46**, 6535; (*e*) O. Moudam, A. Kaeser, B. Delavaux-Nicot, C. Duhayon, M. Holler, G. Accorsi, N. Armaroli, I. Séguy, J. Navarro, P. Destruel and J.-F. Nierengarten, *Chem. Commun.*, 2007, **29**, 3077; (*f*) H. Kunkely, V. Pawlowski and A. Vogler, *Inorg. Chem. Commun.*, 2008, **11**, 1003; (*g*) G. Accorsi, N. Armaroli, B. Delavaux-Nicot, A. Kaeser, M. Holler, J.-F. Nierengarten and A. D. Esposti, *J. Mol. Struct.:THEOCHEM*, 2010, **962**, 7; (*h*) M. F. Cain, S. C. Reynolds, B. J. Anderson, D. S. Glueck, J. A. Golen, C. E. Moore and A. L. Rheingold, *Inorg. Chim. Acta*, 2011, **369**, 55; (*i*) A. Kaeser, M. Mohankumar, J. Mohanraj, F. Monti, M. Holler, J.-J. Cid, O. Moudam, I. Nierengarten, L. Karmazin-Brelot, C. Duhayon, B. Delavaux-Nicot, N. Armaroli and J.-F. Nierengarten, *Inorg. Chem.*, 2013, **52**, 12140; (*j*) J. Yuasa, M. Dan and T. Kawai, *Dalton Trans.*, 2013, **42**, 16096; (*k*) A. Kaeser, O. Moudam, G. Accorsi, I. Séguy, J. Navarro, A. Belbarkra, C. Duhayon, N. Armaroli, B. Delavaux-Nicot and J.-F. Nierengarten, *Eur. J. Inorg. Chem.*, 2014, **8**, 1345; (*l*) M. Viciano-Chumillas, J. M. Carbonell-Vilar, D. Armentano and J. Cano, *Eur. J. Inorg. Chem.*, 2019, **25**, 2982.
5 A. Banerjee, S. Sarkar, J. A. Shah, N. C. Frederiks, E. A. Bazan-Bergamino, C. J. Johnson and M.-Y. Ngai, *Angew. Chem., Int. Ed.*, 2022, **61**, e202113841.
6 P. Saha, M. Jin and D. C.-Y. Huang, *Angew. Chem., Int. Ed.*, 2025, **8**, e202419591.
7 See ESI† for quenching experiments. Also refer to ref. 6 for Stern–Volmer studies with trifluoromethylarenes..
8 (*a*) S. Garakyaraghi, E. O. Danilov, C. E. McCusker and F. N. Castellano, *J. Phys. Chem. A*, 2015, **119**, 3181; (*b*) S. Garakyaraghi, P. D. Crapps, C. E. McCusker and F. N. Castellano, *Inorg. Chem.*, 2016, **55**, 10628;

(*c*) S. Garakyaraghi, P. Koutnik and F. N. Castellano, *Phys. Chem. Chem. Phys.*, 2017, **19**, 16662.

9 Alternatively, the triplet energy can be approximated by using the emission maxima, yielding excited state E_{red} = −1.21 V (complex **1**), −0.68 V (complex **2**), −0.90 V (complex **4**), and −0.78 V (complex **5**) *vs.* SCE in DCE.

10 F. Zhao, W. Zhou and Z. Zuo, *Adv. Synth. Catal.*, 2022, **364**, 234.

11 F. Alonso, I. P. Beletskaya and M. Yus, *Chem. Rev.*, 2002, **102**, 4009.

12 B. Liu, C.-H. Lim and G. M. Miyake, *J. Am. Chem. Soc.*, 2017, **139**, 13616.

13 J. B. I. Sap, N. J. W. Straathos, T. Knauber, C. F. Meyer, M. Médebielle, L. Buglioni, C. Genicot, A. A. Trabanco, T. Noël, C. W. Am Ende and V. Gouverneur, *J. Am. Chem. Soc.*, 2020, **142**, 9181.

14 Z. Burešová, V. Jandová, M. Klikar, M. Grygarová and F. Bureš, *Org. Biomol. Chem.*, 2022, **20**, 9378.

15 B. Michelet, C. Deldaele, S. Kajouj, C. Moucheron and G. Ewano, *Org. Lett.*, 2017, **19**, 3576.